End-to-end 140 GHz Wireless Link Demonstration with Fully-Digital Beamformed System

Shadi Abu-Surra[1], Wonsuk Choi[1], Sungtae Choi[2], Eunyoung Seok[1], Dongjoo Kim[1], Navneet Sharma[1], Siddharth Advani[1], Vitali Loseu[1], Kitaek Bae[2], Ilju Na[2], Ali A. Farid[3], Mark J. W. Rodwell[3], Gary Xu[1], and Jianzhong (Charlie) Zhang[1]

[1] Samsung Research America, Plano, TX, USA
[2] Samsung Research, Samsung Electronics, Seoul, South Korea
[3] ECE Department, University of California, Santa Barbara, CA, USA

Email: {shadi.as, wswill.choi, sungt.choi, dongjoo.k, n1.sharma, s.advani, v.loseu, kitaek.bae, nailju, gary.xu, jianzhong.z}@samsung.com
afarid@ece.ucsb.edu, rodwell@ucsb.edu

***Abstract*— It is projected that mobile traffic will increase by 80x by year 2030. To meet this increase in demand, it is inevitable to utilize the terahertz bands (0.1 THz to 10 THz) for future 6G wireless systems. However, operating at such high frequency comes with several fundamental and technical challenges. In this work, we present a proof-of-concept system to demonstrate the feasibility of establishing a communication link at 140 GHz carrier frequency. In addition, this work highlights techniques to tackle the challenges that comes with operating in the terahertz regime. To the authors knowledge, this is the world's first end-to-end system with up to 16-channel digitally-beamformed 140 GHz system and dynamic beam steering capability. The paper presents lab results which demonstrate link throughput of 6 Gbps at 15-meter distance with adaptive beamforming.**

Keywords—Terahertz, wireless, prototype, beamforming.

I. INTRODUCTION

It is inspiring to note that in March 2019, the Federal Communications Commission (FCC) opened the spectrum between 95 GHz and 3,000 GHz for experimental use and unlicensed applications, to encourage the development of new wireless communication technologies [1]. Moreover, discussions on use cases and deployment scenarios for 5G NR systems operating beyond 52.6 GHz bands have already begun, and support for operation in these bands will be included in 3GPP Release 16 [2]. Following this trend, it is inevitable that telecommunications will utilize the terahertz (THz) bands for future wireless systems. The THz band is here defined as the frequencies ranging from 0.1 THz to 10 THz, which aligns with some publications such as [3]. A total of 102 GHz spectrum in the range between 95 GHz and 300 GHz is being made accessible for licensed fixed point-to-point and mobile services through the Spectrum Horizon program [4]. Accordingly, the extremely wideband THz channels with tens of GHz-wide bandwidth could potentially support the Tbps communication envisioned by the future 6G standard. Samsung envisions that the THz communications will play an essential role in enabling terabit-fast speed (i.e., terabit-per-second throughput) in future 6G systems [5].

One may argue why do we need terabit-fast data rate for our devices in the future. The simple answer: there is no limit to human creativity, if we provide such a wide data pipe, the innovators will utilize it in extremely creative ways beyond today's imagination. Nevertheless, there are many trends that indicate an increase in the demand for throughput in the near future. Of these trends, fast growth in artificial intelligence (AI), robotics, and automation is anticipated. In this vision, machines will be the dominant consumers of the communication networks. Having terabit-fast links will enable the sheer number of machines to mesh network without bottlenecks. Moreover, some of these machines might take the form of a truly immersive extended reality (XR), high-fidelity mobile hologram, or digital replica [5]. These high-end machines will require communication links with terabit-fast speeds.

To realize stable THz communications in practice is not straight forward, and a handful of fundamental and technical challenges need to be overcome. Commonly, this band is often referred to as the terahertz gap that is mainly due to the lack of efficient devices, which generate and detect signals in these frequencies. In this band the device dimensions are significant relative to the signal wavelength, and this results in high losses by dielectric loss and skin-depth, surface roughness losses. Also devices show low efficiency by significant impact of parasitics of the device. The severe path-loss and atmospheric absorption add to the challenge of utilizing this band. On the positive side, in the past 10 years a lot of research and development have been done on: 1) designing RF circuits operating at the lower THz band [6], and 2) utilizing large antenna arrays to mitigate path-loss. Scaling up this technology to extremely large phased arrays will be essential to realize a reliable THz link.

In this paper, a proof-of-concept (PoC) to demonstrate the feasibility of building a wireless link at the lower THz band, specifically at 144 GHz carrier frequency is presented. In the following section, the overall system description is presented. In Section III, the RF specifications are shown. In Section IV, the baseband modem specification and design are shown. In Section V, the system architecture and signal processing are explained. In Section VI, the experimental setups are shown, and the lab measurement results are presented.

II. Overall System Description

The overall system setup is shown in Fig. 1. In this system, the data is generated by the host-PC at the transmitter side, sent to the modem (baseband and data-convertors), then to the RF unit. One of the following RF units are used at the transmitter side: a) Fixed-beam RF, which consists of the Keysight I/Q modulator, VDI up-convertor, and lens antenna. b) TX-beamformer RF, which is described in the following section. The transmitted signal is picked up by the receiver RF, which down-converts the signal to baseband. The baseband signal is digitized then processed by the digital beamformers and the baseband modem. Finally, the recovered data is sent to the host-PC at the receiver side. Further details of the baseband modem, digital beamformers, and RF-units are provided in the next few sections.

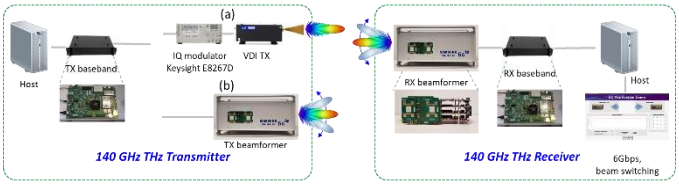

Fig. 1. Overall end-to-end system setup with fixed beam Tx in (a) and Tx beamformer in (b).

III. RF Specifications

At the transmitter side, two RF options were used. First, the fixed-beam RF, which is based on the VDI up-convertor module. Second, the TX beamformer, which is based on the 45nm CMOS RFICs developed by the Univ. of California, Santa Barbara (UCSB) [7].

In the fixed-beam RF, the I/Q baseband signal is up converted to an intermediate frequency (IF) using the Keysight E8267D. The IF is then up-converted to 144 GHz RF frequency using the VDI module. The VDI module consists of an up-convertor and a power-amplifier (PA), and provided an output power of -4 dBm. Note, at this output power the module operates at about 10 dB back off from saturation, which provides good linearity for 16-QAM single-carrier waveform. The PA output is then filtered and transmitted using a 42 dBi lens-antenna. The transmit effective isotropically radiated power (EIRP) for this unit is 35 dBm.

In the TX beamformer, the I/Q baseband signal is replicated 16 times, each replica is rotated using the digital phase-shifter, processed to apply the transmitter I/Q imbalance and phase calibration, then fed to the digital-to-analog convertor (DAC). Note that this part is implemented using four Xilinx ZU28DR RFSoC, called digital RF FPGA, where each FPGA processes four I/Q channels. The system architecture is shown in Fig. 2. The I/Q channels are then directly up-converted to 144 GHz using the 45nm CMOS TX RFIC. Each RFIC has two channels, 18-22dB of I/Q imbalance or image rejection, LO suppression of 22-25 dB, output power of -3 dBm per channel (-6 dBm at the input of the antenna after wire bonding), and measured EVM of -14 dB. Note that this RFIC has limiters at the I and Q inputs, and so -14 dB EVM is expected. This limits the use of this RFIC to QPSK single-carrier waveform. The detailed specifications of the RFIC are in [7]. The TX beamformer module, made using conventional PCB fabrication process, is shown in Fig. 3 carrying the RFICs and the antenna array. A zoom-in view on the RFIC wire-bonded to the board is shown in Fig. 4.

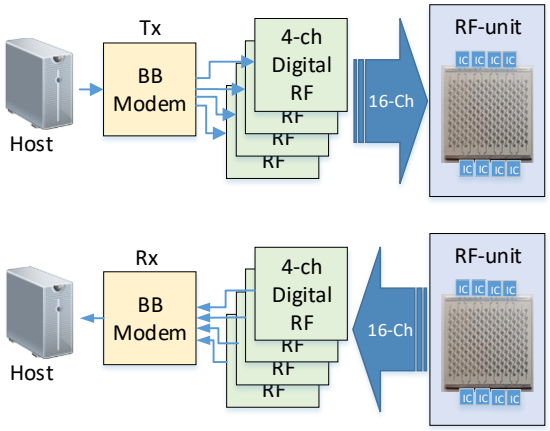

Fig. 2. System architecture for transmitter and receiver digital beamformers.

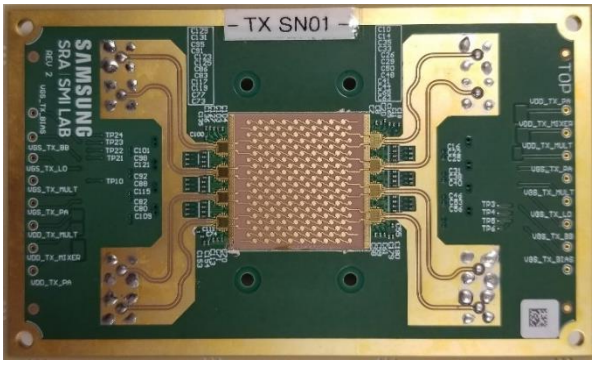

Fig. 3. The TX beamformer module with eight dual-channel 144GHz RFICs wire bounded to the antenna array.

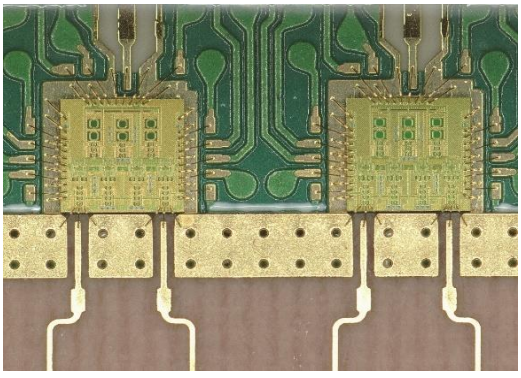

Fig. 4. Zoom-in view of the RFICs wire bounded to the antenna array and the TX beamformer module.

The RX beamformer has similar structure as that of the TX. The 144 GHz is directly down-converted to the I/Q baseband signal using the CMOS RX RFIC from UCSB [8]. A total of eight RFICs are used, each has two channels. The conversion

gain for this RFIC is 12 dB, and the noise figure is 10 dB. The I/Q signals are sampled using the 4 Gsps analog-to-digital convertors (ADC) on the digital RF board (see, the architecture in Fig. 2). The digitized signals are rotated using digital-phase shifter, then combined and passed to the baseband modem.

A 128-element antenna array, made using regular PCB fabrication process, is used at the TX beamformer, and a similar array is used at the RX beamformer. The array is developed to achieve 21 dBi gain with a scanning range of +/-40 degree in azimuth direction. The array is shown in Fig. 5, and compared in size to the size of a US penny. The simulated beam patterns of the array steered in different azimuth angles are shown in Fig. 6. The array includes 20 sub-arrays. 16 of these sub-arrays are driven by the RF chains, while the other 4 sub-arrays (two at each side) are dummy subarray to keep the symmetry for the edge sub-arrays. Each sub-array consists of 8 radiating patch antennas plus a termination element. The elements of the sub-array are serially fed circular patches with insets. Note the array has 180 elements, but only 128 elements are radiating elements.

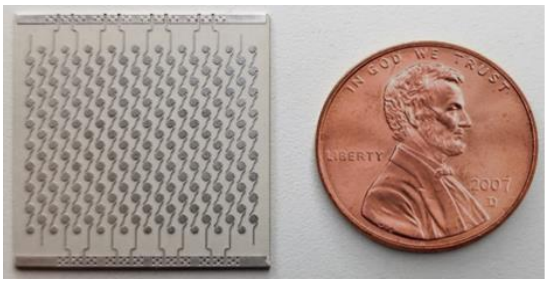

Fig. 5. Antenna array with 16 RF channels at 144 GHz carrier frequency.

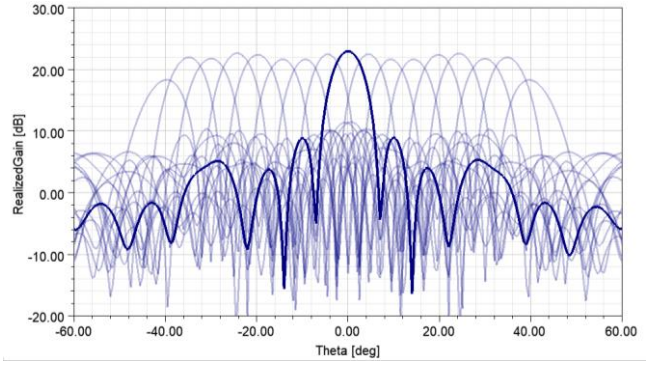

Fig. 6. Antenna pattern shows 21 dB of realized gain and +/-40 degree steerability.

TABLE I shows the link-budget for three different variations of the setup. In the first setup (labeled: 4-Ch), four beamformed channels are used at the TX and four at the RX. The TX beamformer can provide EIRP of 17 dBm. This can support a spectral efficiency of 2.06 b/s/Hz at a distance of 5 meters. In the second setup (labeled: 16-Ch), sixteen beamformed channels are used at the TX and sixteen at the RX to achieve EIRP of 27 dBm. This EIRP can support a spectral efficiency of 3.16 b/s/Hz at a distance of 15 meters. In the third setup (Labeled: Lens), the fixed-beam RF is used at the transmitter side, and eight beamformed channels are used at the Rx side. This transmit module provides EIRP of 35 dBm, which can support a spectral efficiency of 5 b/s/Hz at a distance of 15 meters.

In the spectral efficiency calculations, the line-of-sight (LoS) free-space path-loss model is used, which is given by:

$$PL = 32.45 + 20\log(d) + 20\log(f),$$

where d is distance in meter, and f is the frequency in GHz. Moreover, the Shannon capacity formula is used after applying a margin of 10 dB for other losses. These losses include algorithmic losses in the baseband modem, but more importantly it also accounts for hardware impairments, losses due to routing the 144 GHz signal between the RFIC and the antennas, and the imperfections in the array calibration.

TABLE I. SYSTEM LINK-BUDGET

Parameter	4-Ch	16-Ch	Lens
RF Frequency (GHz)	144	144	144
Bandwidth (GHz)	2	2	2
Number of RF TX Channels	4	16	1
Number of RF RX Channels	4	16	8
RFIC TX Output Power (dBm/PA)	-6	-6	-4
TX Antenna Gain (dBi)	17	21	42
RX Antenna Gain (dBi)	17	21	19
EIRP (dBm)	17	27	35
RX LNA Noise Figure (dB)	10	10	10
Distance (m)	5	15	15
Path-Loss (dB)	90	100	100
Margin for other TX/RX losses (dB)	10	10	10
Max. spectral efficiency [b/s/Hz]	2.06	3.16	5.02
Theoretic max. throughput [Gbps]	4.1	6.3	10
Modulation	QPSK	QPSK	16-QAM
Achieved throughput [Gbps]	3.19	-	6.39

IV. BASEBAND MODEM SPECIFICATIONS

The baseband modem implements a single-carrier waveform, and has the frame structure in Fig. 7. Each frame is 25 *ms* in length and consists of a 1 *ms* beamforming training session and 24 *ms* data session.

The beamforming training session includes 640 beamforming training intervals (BFTI). Out of the 640 BFTI, the first 13 BFTI and the last 2 BFTI were set to Null BFTI (i.e., send zeros). Effectively, 625 BFTI were actually used. These BFTI are used to test for all the combinations of 25 transmit-beams and 25 receive-beams every 25 *ms* using exhaustive search algorithm. The beamforming procedure is as follows: the transmitter sends 25 consecutive BFTIs on the same beam before switching to the next beam. On the receiver side, the Rx cycle its beam each BFTI, and it keeps track of the beam pairs, which maximizes the RSSI to be used in the data-session of the next frame. This procedure is shown in Fig. 7.

The data session consists of 120 data-slots. Each data-slot is 200 μs long to allow fast channel tracking and equalization. The data-slot structure is shown in Fig. 8. It starts with a null of length 3808 zeros. This null period is used to estimate the noise on the channel, and has practical benefits in a prototyping

system such as relaxing the timing constraints on the system. Next is the channel estimation field (CEF), which is shown in Fig. 8. The CEF is constructed using complimentary Golay sequences and has the same structure as in IEEE802.11ay [9]. The CEF has a zero-correlation zone of length 130 *ns*, which is estimated to be long enough to accommodate the delay spread of the channel. The CEF is followed by 758 single-carrier blocks (SC-Block). Each SC-Block is 512 Chips long, of them 480 are data symbols (data-block), and 32 are guard-pilot symbols (guard-block). The guard-block is used to facilitate frequency-domain equalization and to track phase-noise.

The waveform supports the following modulation and coding schemes (MCS): 1) QPSK with rate-1/2 LDPC code. 2) QPSK with rate-11/12 LDPC code. 3) 16-QAM with rate-11/12 LDPC code. The code bit error rate curves for these MCSs are shown in Fig. 9. The throughput achieved by these MCSs is 1.74, 3.19, and 6.39 Gbps, respectively, after accounting for all system overhead.

The waveform numerology is depicted in TABLE II. Note, the waveform chip-rate is 1.96608 G Chip/s, and it is filtered using a root-raised-cosine (RRC) filter with roll-off factor 0.2. And so, the waveform occupies 2.36 GHz of bandwidth after filtering. However, when the TX beamformer is used, spectral regrowth is observed, which is expected, due to the limiters at the RFIC inputs. Also note, the guard-block accommodates for a channel delay spread of 16 *ns*, and has a periodicity of 260.42 *ns*. This periodicity allows for tracking about 500 KHz of phase-noise as shown in Fig. 10.

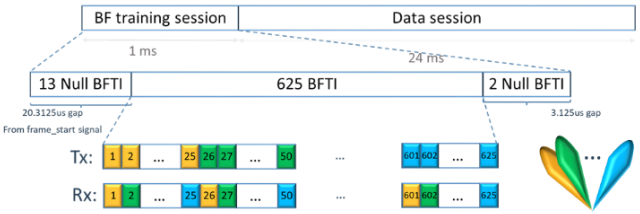

Fig. 7. Single-carrier waveform's frame structure and beam cycling proceedure during BF training session.

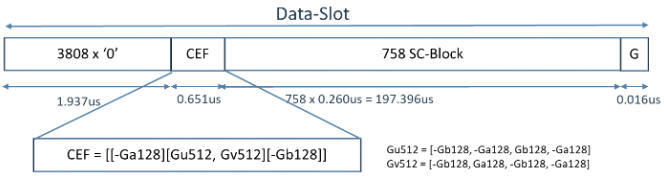

Fig. 8. Data-Slot structure in the data session and CEF structure.

TABLE II. SINGLE-CARRIER WAVEFORM NUMEROLOGY.

Parameter	Value	Unit
Chip-Rate	1.96608	G Chip/s
Chip-Duration	0.508626302	*ns*
SC-Block length	512	Chip
Guard-block length	32	Chip
Data-block length	480	Chip
Guard-block duration	16.27604167	*ns*
Data-block duration	244.140625	*ns*
SC-Block duration	260.4166667	*ns*

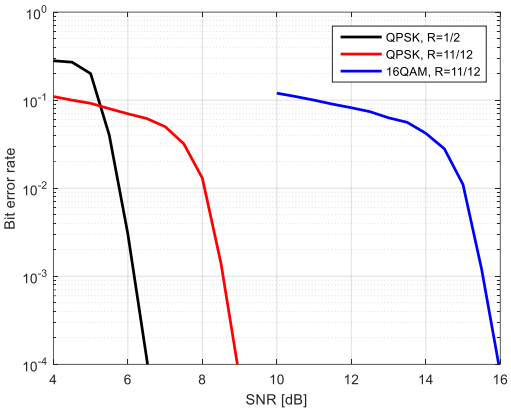

Fig. 9. Coded bit error rate verses SNR for the different MCSs.

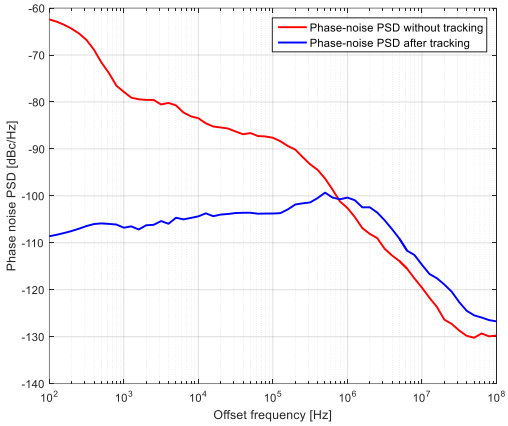

Fig. 10. Phase-noise power spectrum density before and after tracking.

V. SYSTEM ARCHITECTURE

The system architecture is shown in Fig. 2. The processing of the information bits is described, as they flow from the TX host PC to the RX host PC.

On the transmitter side: The host PC generates traffic, and sends it over Ethernet to the baseband modem FPGA. The baseband modem encodes the data, then sends four similar copies over CPRI to the four digital RF FPGAs. Each one of these FPGAs modulates the data, constructs the frames, then resamples and filters the signal using a root-raised-cosine (RRC) filter with roll-off factor 0.2. After that, the signal is replicated four times, each replica is rotated using the digital phase-shifter, processed to apply the transmitter I/Q imbalance and phase calibration, then fed to the DACs. Finally, the analog I/Q signals are sent to the RF-units.

On the receiver side: The analog baseband signals form the RF-unit are digitized using the ADCs in the digital RF FPGA, four channels at each FPGA. Each channel is corrected for I/Q imbalance and phase-mismatch, then rotated using digital-phase shifters according to a preloaded beamforming table. The four channels are then combined, filtered using the matching filter. The output of the matching filter is then passed to the synchronization module, channel estimation module, equalizer. The synchronization module signals the start of a CEF in a data-

slot to the channel estimation module. The channel estimation module captures the received CEF and estimates the channel, then passes the estimation to the equalizer. The equalizer converts the time-domain channel to the frequency domain using 512 FFT, then uses it to equalize the received SC-block one-by-one in the frequency domain. The equalizer implements a fractionally spaced equalizer (FSE) with 2x oversampling to alleviate the receiver sensitivity to sampling offset impairment. More details on the used equalizer can be found in [10]. The equalized symbols are processed using the phase-noise tracking module, which corrects for the common phase-error in the SC-block. The output of the phase-noise module is sent to the baseband modem FPGA, which averages the corresponding four symbols from the four digital RF boards, demodulates the averaged symbols into soft log-likelihood-ratios (LLRs), decodes the LLRs and recovers the information bits, packages the data into IP packets, then sends them to the host PC at the receiver side.

VI. System Setup and Lab Measurements Result

In this section two prototyping setups are presented. The 4-Ch TX and 4-Ch RX beamformers setup, and the Lens TX and 8-Ch RX beamformer setup.

A. *Setup 1: 4-Ch TX and 4-Ch RX beamformers*

The setup is in Fig. 11. Both transmitter and receiver were setup on a lab bench about 1 meter apart from each other. To emulate a larger distance between the transmitter and the receiver, absorbent material was added in the LoS path between them. A removable metal plate was used as a blocker for the LoS path. Moreover, a metal reflector was placed to emulate a second path between the transmitter and the receiver.

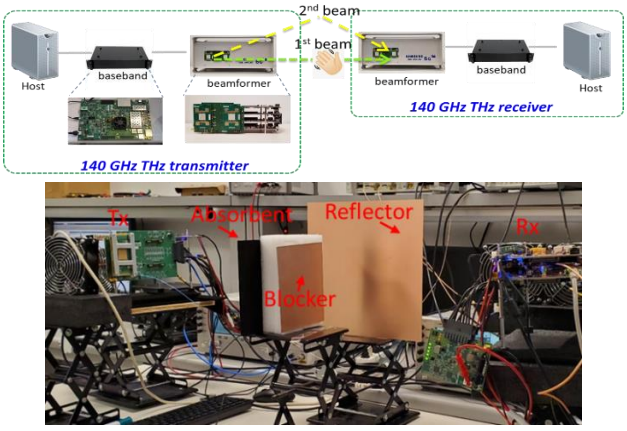

Fig. 11. 4-Ch TX and 4-Ch RX beamforming setup.

Recall, the TX RFICs have limiters at the I/Q inputs, which limited our end-to-end experiments to QPSK modulation. Consequently, the beam switching demo was conducted using QPSK rate-11/12 MCS, which achieves a maximum throughput of 3.19 Gbps. The scenario is as follows: The system was started without blocking the LoS path (i.e., without the blocker plate), the link was established using a 1st beam, then the blocker plate was placed to block the LoS path. As a response the system switched the beam to reestablish the link using a 2nd beam via the reflected path.

Fig. 12 shows the measured SNR and EVM while sweeping the Rx beam. Here, the blocker and reflector plates were removed, and the TX beam was kept fixed at beam-index zero (i.e., along the LoS path toward the receiver). Note that the estimated maximum SNR is 28 dB, which was achieved with RX beam-index zero. However, the maximum achieved EVM is -14 dB, which was limited by the non-linearity of the TX RFIC.

The measurements were repeated after placing the blocker and reflector plates. Fig. 13 shows the results. Note, the drop in the maximum SNR from 28 dB to 13 dB. Also the maximum EVM was limited to -8.7 dB using a beam pointing to the edge of the blocker from the reflector side. After that, the TX-beam was switched to beam index 11, toward the reflector plate. The results of the RX-beam sweep are shown in Fig. 14. The SNR recovered to 25 dB when the RX was pointing its beam toward the reflector.

Fig. 15 shows the throughput results at the different stages of the experiment. The throughput was 3.15 Gbps during the first 37 seconds with LoS link, then the blocker plate was added. As a result, the link was dropped. Once the TX and RX beams were switched to point to the reflector, the link recovered and achieved throughput of 3.15 Gbps. At 75 seconds, the beam was switched back to the LoS direction, which caused the link to drop until the blocking plate was removed.

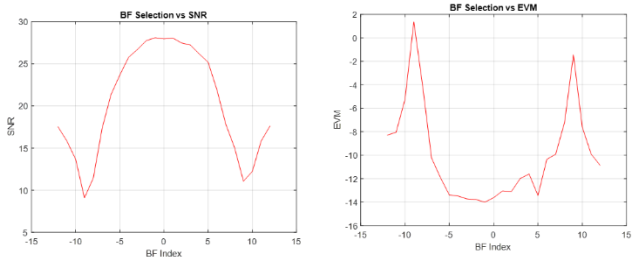

Fig. 12. SNR and EVM Measurement as a function of Rx beam sweep in LoS link.

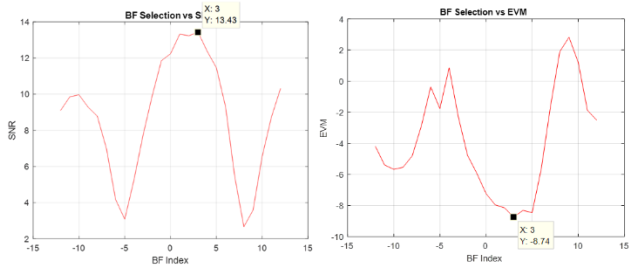

Fig. 13. SNR and EVM Measurement as a function of Rx beam sweep with blocker and reflector, and Tx-Beam 0.

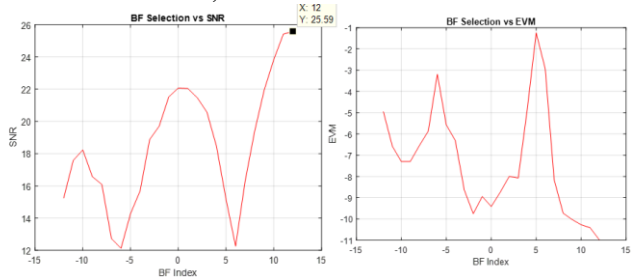

Fig. 14. SNR and EVM Measurement as a function of Rx beam sweep with blocker and reflector, and Tx-Beam 11.

Fig. 15. Demonstrating 3 Gbps link with beam steering.

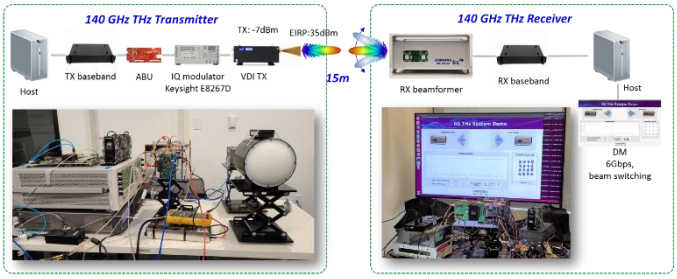

Fig. 16. Lens TX and 8-Ch RX beamformer setup.

B. *Setup 2: Lens TX and 8-Ch RX beamformer setup.*

The setup is shown in Fig. 16, the TX and RX were placed at a distance of 15 meters apart with clear LoS. The link achieved an EVM of -18 dBm, which was sufficient to operate the link at 6.3 Gbps using the 16-QAM rate-11/12 MCS.

To demonstrate the adaptive beamforming at the RX side, the RF-unit was placed on a manual rotation stage, and data-rate performance was compared when the adaptive beam-steering was enabled to that when it was disabled. The results are shown in Fig. 17. Large fluctuation in data rate (0 to 6.3 Gbps) was observed rotating the RX ±30° with disabled adaptive beam-steering. On the other hand, the data rate stayed above 6 Gbps, when this experiment repeated with the adaptive beamforming enabled.

Fig. 17. Data-rate performance while rotating the RX ±30° with adaptive beamforming disabled in (a) and enabled in (b).

Fig. 18 shows the RSSI for the different BFTI indices, when the RX is facing the TX, and when it is rotated 10° counter clockwise from the direction facing the TX. Note that only the first 25 BFTI are shown. The pattern repeats after that, as the TX beam is fixed.

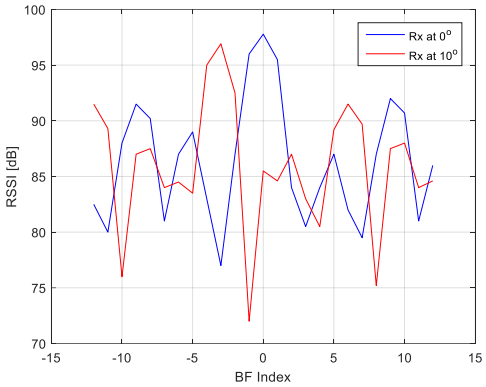

Fig. 18. RSSI vs BF codeword index when the RX broad-side beam is facing the TX (blue), and when the RX is rotated 10° counter clockwise from the direction facing TX.

VII. Conclusion

In this paper, a 144 GHz wireless link prototype is presented to demonstrate the feasibility of lower THz bands for wireless communications. The prototype showed a real-time link with adaptive beam steering, which provided data-rate of 6.3 Gbps at 15-meter distance in a 2 GHz of bandwidth. These are promising results at this stage. On the other hand, they highlight the challenge ahead before realizing a practical system.

Acknowledgment

The authors would like to thank Global Foundries for the 45 nm CMOS SOI chip fabrication.

References

[1] FCC Docket 18-21, "FCC opens spectrum horizons for new services and technologies," Mar. 2019.
[2] 3GPP TR 38.807-010, "Study on NR beyond 52.6 GHz," Mar. 2019.
[3] Roger D. Pollard, "Guest Editorial," IEEE Transactions on Microwave Theory and Techni ques, vol. 48, no. 4, pp. 625-625, Apr. 2000.
[4] FCC 19-19 First Report and Order, "Spectrum horizons," Mar. 2019
[5] Samsung white-paper, "Samsung 6G vision," Jul. 2020, https://cdn.codeground.org/nsr/downloads/researchareas/6G%20Vision.pdf
[6] Kaushik Sengupta et al., "Terahertz integrated electronic and hybrid electronic–photonic systems" Nature Electron, vol. 1, no. 12, pp. 622-635, Dec. 2018.
[7] Arda Simsek, Ahmed S. H. Ahmed, Ali A. Farid, Utku Soylu and Mark J. W. Rodwell, "A 140GHz Two-Channel CMOS Transmitter using Low-Cost Packaging Technologies", IEEE Wireless Communications and Networking Conference, May 2020.
[8] A. Simsek, S. Kim and M. J. W. Rodwell, "A 140 GHz MIMO Transceiver in 45 nm SOI CMOS," 2018 IEEE BiCMOS and Compound Semiconductor Integrated Circuits and Technology Symposium (BCICTS), San Diego, CA, 2018, pp. 231-234.
[9] IEEE draft standard for information technology - telecommunications and information exchange between systems local and metropolitan area networks - specific requirements part 11: Wireless LAN Medium Access Control (MAC) and Physical Layer (PHY) Specifications, IEEE P802.11ay/D5.0, October 2019.
[10] Qiaoyang Ye, Joonyoung Cho, Jeongho Jeon, Shadi Abu-Surra, Kitaek Bae, and Jianzhong Zhang, "Fractionally Spaced Equalizer Design for Terahertz Wireless Communication Systems" Submitted to IEEE ICC 2021 Workshop - TeraCom.